J. Meas. Sci. Instrum., 2025, 16(2): 161-172. http://jmsi.publish.founderss.cn/
DOI: 10.62756/jmsi.1674-8042.2025016 jmsi@nuc.edu.cn

Non-contact radar-based HRV monitoring method using adaptive cycle segmentation and peak extraction

GAO Yixuan[1], ZHU Xinxing[1], LI Mingchao[1], WU Enkang[1], GU Xiaofeng[1], WANG Cong[2], YU Tian[1*], LIANG Junge[1,3,4*]

1. School of Integrated Circuits, Jiangnan University, Wuxi 214122, China;
2. School of Electronics and Information Engineering, Harbin Institute of Technology, Harbin 150001, China;
3. RFIC Center, Kwangwoon University, Seoul 01897, Republic of Korea;
4. Department of Medical and Digital Engineering, Hanyang University, Seoul 04763, Republic of Korea

***Corresponding authors:** LIANG Junge (liangjunge@hotmail.com); YU Tian (yutian@jiangnan.edu.cn)

Received: May 22, 2025 **Revised:** June 6, 2025 **Accepted:** June 10, 2025

Abstract: Heart rate variability (HRV), as a key indicator for evaluating autonomic nervous system function, has significant value in areas such as cardiovascular disease screening and emotion monitoring. Although traditional contact-based measurement methods offer high precision, they suffer from issues such as poor comfort and low user compliance. This paper proposes a non-contact HRV monitoring method using frequency modulated continuous wave (FMCW) radar, highlighting adaptive cycle segmentation and peak extraction as core innovations. Key advantages of this method include: 1) effective suppression of motion artifacts and respiratory harmonics by leveraging cardiac energy concentration; 2) precise heartbeat cycle identification across physiological states via adaptive segmentation, addressing time-varying differences; 3) adaptive threshold adjustment using discrete energy signals and a support vector machine (SVM) model based on morphological-temporal-spectral characteristics, reducing complexity while maintaining precision. Previous approaches predominantly process radar signals holistically through algorithms to uniformly extract inter-beat intervals (IBIs), which may result in high computational complexity and inadequate dynamic adaptability. In contrast, our method achieved higher precision than conventional holistic processing approaches, while maintaining comparable precision with lower computational complexity than previous optimization algorithms. Experimental results demonstrate that the system achieves an average IBI error of 8.28 ms (RMSE of 15.3 ms), which is reduced by about 66% compared with the traditional holistically peak seeking method. The average errors of SDNN and RMSSD are 2.65 ms and 4.33 ms, respectively. More than 92% of the IBI errors are controlled within 20 ms. The distance adaptability test showed that although the accuracy of long-distance measurement decreased slightly (<6 ms), the overall detection performance remained robust at different distances. This study provided a novel estimation algorithm for non-contact HRV detection, offering new perspectives for future health monitoring.

Key words: HRV; FMCW radar; cycle segmentation; adaptive threshold; non-contact monitoring

0 Introduction

Heart rate variability (HRV), as a critical physiological indicator for evaluating autonomic nervous system function, has shown significant value in various fields such as cardiovascular disease screening, emotional state monitoring, and stress level analysis. By quantifying dynamic variations in successive heartbeat intervals, HRV reflects the human body's complex physiological regulatory mechanisms and latent pathological information[1,2]. For instance, the LF/HF ratio demonstrates high diagnostic sensitivity for detecting early-stage autonomic dysfunction in diabetic neuropathy screening[3]. While in clinical mental health assessment, RMSSD magnitude correlates significantly with acute stress states[4]. Traditional contact-based measurement methods widely adopted in clinical practice, such as electrocardiography (ECG) and photoplethysmography (PPG)[5], although highly accurate, require the sensor to be directly attached to the human body, which not only restricts the user's freedom of movement, but also may cause skin irritation and discomfort during long-term use, thereby reducing the voluntary monitoring compliance of patients[6].

Non-contact HRV monitoring technology has overcome these limitations, enabling continuous physiological parameter measurement in natural and comfortable environments. Existing non-contact vital sign detection technologies include thermal imaging[7], remote

photoplethysmography (rPPG)[8], laser doppler vibrometry (LDV)[9], and ultrasonic technology[10]. However, these methods exhibit notable constraints. For example, thermal imaging and rPPG are susceptible to environmental lighting and temperature fluctuations; Imaging based techniques inevitably raise privacy concerns, limiting their acceptance in personal and medical settings[11]; High-precision methods such as LDV remain cost-prohibitive and operationally complex for widespread implementation; While ultrasonic technology has limitations in spatial resolution and is less effective for dynamic physiological monitoring[12]. In contrast, monitoring methods based on radio frequency (RF) technology can effectively avoid these limitations and demonstrate unique advantages.

Common RF vital sign monitoring technologies include 2.4/5 GHz Wi-Fi signal analysis[13], continuous wave (CW) Doppler radar[14], and ultra-wideband (UWB) pulse radar[15]. These technologies are not affected by external environmental factors such as lighting, acoustic noise, or temperature fluctuations, etc., offering superior penetration capabilities while preserving user privacy. However, Wi-Fi technology exhibits limitations in accuracy and response time, CW radar demonstrates excessive sensitivity to ambient noise, while UWB radar's constrained ranging accuracy struggles to meet the precision requirements for measuring subtle parameters like HRV. Frequency modulated continuous wave (FMCW) radar technology, with its excellent range resolution and signal stability, not only retains the shared advantages of RF techniques but also provides enhanced measurement precision. Especially in application scenarios such as sleep quality assessment, multi-target ward monitoring, and chronic disease management for elderly patients, FMCW radar technology has demonstrated significant potential[16-19].

However, accurate extraction of HRV information from radar reflection signals still faces many challenges, primarily including low signal-to-noise ratio (SNR), motion artifact interference, and signal characteristic variations caused by individual differences. To address these issues, research teams have proposed various processing methods to improve the accuracy of HRV extraction. Hosseini et al.[20] innovatively employed discrete prolate spheroidal sequences (DPSS) to construct time-varying filters, which reduced HRV extraction interference through estimation of stochastic body movement phase signals. Hu et al.[21] employed wavelet transform combined with ensemble empirical mode decomposition (EEMD) to separate cardiac and respiratory signals, focusing on identifying an optimal wavelet basis through spectral correlation analysis, thereby optimizing heartbeat signal extraction. Wang et al.[22] leveraged whole-body reflections and modeled intrinsic spatiotemporal relationships between these reflections and cardiac activity through deep neural networks, achieving a 20% reduction in IBI error with a median IBI error of 12 ms. Yuan et al.[23] designed a sophisticated deep learning network incorporating residual channel attention block (RCAB) to enhance feature extraction and suppress respiratory harmonic interference. Han et al.[24] combined minimum variance distortionless response (MVDR) beamforming to suppress interference, amplified heartbeat signals through second derivative computation of chest motion signals, and dynamically adjusted segmentation points via joint optimization algorithms to extract heartbeat intervals, attaining a root mean square error (RMSE) of 14.9 ms for IBI. Zhang et al.[25] exploited the faster attenuation characteristics of respiratory harmonics at high frequencies to extract cardiac higher-order harmonics, decoded heartbeat signals through differential frequency effects, and employed variational mode decomposition (VMD) for heartbeat pattern extraction, achieving approximately tenfold improvement in precision compared to baseline methods. However, most existing approaches holistically process signals over time windows through algorithms, which may extract cardiac signals but suffer from high computational complexity and limited dynamic adaptability.

This paper proposes a non-contact FMCW radar-based HRV monitoring method based on adaptive cycle segmentation and peak extraction. Compared with traditional holistic signal processing methods, the core advantages of this method lie in: 1) effectively suppressing motion artifacts and respiratory harmonic interference through second derivative and nonlinear compression by utilizing the strong energy concentration characteristics of cardiac events; 2) achieving more precise identification of heartbeat cycles under different physiological states through adaptive cycle segmentation, effectively addressing individual differences and time-varying characteristics; 3) adopting discrete energy signals combined with a support vector machine (SVM) algorithm based on morphological-temporal-spectral characters to adaptively adjust signal processing thresholds, which reduces computational complexity while maintaining the precision of heartbeat cycle segmentation.

1 Theoretical model and system overview

1.1 FMCW radar signal model

FMCW radar system transmits linear frequency modulated (LFM) pulse signal and receives the signal

reflected along the transmission path[26-28]. With its operating frequency typically in the GHz range, directly sampling and processing these high-frequency signals will require high-bandwidth analog-to-digital converters (ADCs) and complex circuitry, which results in both high costs and significant technical challenges. By mixing the received signal with the transmitted signal to generate the beat signal, the high-frequency echo signals can be converted to intermediate frequency (IF) signals, thereby significantly reducing the complexity of signal processing hardware. Fig.1 illustrates a simplified block diagram of the radar's main RF components.

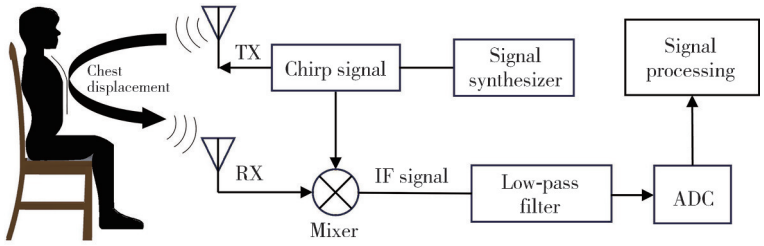

Fig. 1 FMCW radar composition block diagram

First, an initial LFM signal is generated by the synthesizer. If the FMCW system's initial frequency is f_0 and the pulse width is T, the instantaneous frequency $f(t)$ of the signal changes linearly with time, i.e.,

$$f(t)=f_0+\mu t,\ 0\leqslant t\leqslant T, \tag{1}$$

where μ is the chirp rate, defined as the ratio of bandwidth B and pulse width T, with unit of Hz/s. This parameter determines the linear relationship between the frequency and target distance, where a larger chirp rate yields higher range resolution. The phase $\phi(t)$ of the LFM signal is the integral of the instantaneous frequency, that is

$$\phi(t)=2\pi\int_0^t f(\tau)\mathrm{d}\tau+\varphi_0=2\pi\left(f_0t+\frac{\mu}{2}t^2\right)+\varphi_0, \tag{2}$$

where φ_0 is the initial phase of the signal. Therefore, the time domain expression of LFM signal is

$$S_{\mathrm{T}}(t)=A_{\mathrm{T}}\cos\left[2\pi\left(f_0t+\frac{\mu}{2}t^2\right)+\varphi_0\right], \tag{3}$$

where A_{T} is the amplitude of the transmitted signal. The LFM pulse is transmitted by the transmitting antenna (TX antenna). When the TX signal is reflected by the human chest at $d(t)$, the signal $S_{\mathrm{R}}(t)$ received by the radar can be expressed as

$$S_{\mathrm{R}}(t)=A_{\mathrm{R}}\cos\left[2\pi f_0(t-\tau)+\pi\mu(t-\tau)^2+\varphi_0\right], \tag{4}$$

where A_{R} is the amplitude of the received signal (RX signal), and the signal delay time $\tau=2d(t)/c$, where c represents the speed of light.

Next, the mixer combines RX and TX signals to generate an IF signal (as shown in Fig.2). The generated IF signal can be expressed as

$$h(t)=\frac{1}{2}A_{\mathrm{T}}A_{\mathrm{R}}\mathrm{e}^{\mathrm{j}\left(2\pi\frac{B_\tau}{T_c}t+2\pi f_0\tau-\pi\frac{B}{T_c}\tau^2\right)}, \tag{5}$$

$$\phi_b(t)=2\pi f_0\tau-\pi\frac{B}{T_c}\tau^2, \tag{6}$$

where $\phi_b(t)$ represents the phase change due to the time delay caused by distance. In practical application, since $c^2\gg\left[d(t)^2\right]$, the term $\pi\left(B/T_c\right)\tau^2$ can be ignored, therefore the IF signal can be written as

$$h(t)=\frac{1}{2}A_{\mathrm{T}}A_{\mathrm{R}}\mathrm{e}^{\mathrm{j}\left(2\pi\frac{B_\tau}{T_c}t+2\pi f_0\tau\right)}. \tag{7}$$

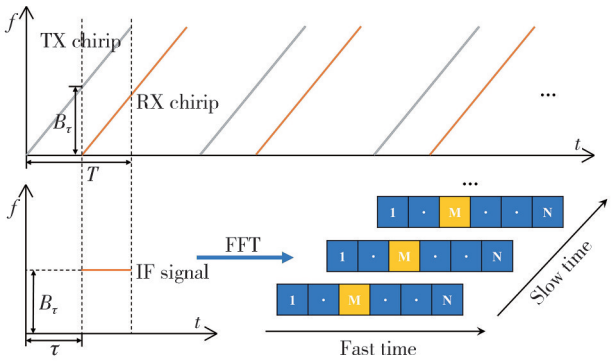

Fig. 2 FMCW radar system

In an FMCW radar system, the transmitted chirp waveform is reflected by the target, and its baseband signal $h(t)$ is converted into a discrete digital sequence through ADC operating at a fixed sampling rate. For a single LFM pulse, the system acquires N uniformly distributed sampling points in the time domain according to the Nyquist sampling theorem. The discrete time dimension formed by this process is called fast time dimension, whose temporal resolution is determined by the ADC sampling frequency f_s. In the slow time dimension, the radar sequentially transmits M chirp pulse sequences with a period T_c, where the start time of each chirp constitutes the slow time sampling points $t_m=mT_c(m=0,1,\cdots,M-1)$. Therefore, the IF signal can also be expressed as

$$h(n,m)=\frac{1}{2}A_{\mathrm{T}}A_{\mathrm{R}}\mathrm{e}^{\mathrm{j}\left(2\pi\frac{B_\tau}{T_c}nT_{\mathrm{f}}+\frac{4\pi d(nT_{\mathrm{f}}+mT_{\mathrm{s}})}{\lambda_c}\right)}, \tag{8}$$

where n and m denote the nth ADC sample in the fast time dimension and the mth chirp in the slow time dimension; T_{f} and T_{s} represent the fast time and slow time intervals; λ_c is the wavelength of the chirp; $d(nT_{\mathrm{f}}+mT_{\mathrm{s}})$ indicates the

distance between the radar and the target.

1.2 Relationship between radar signal and HRV

As a reflection of the periodicity of vital signs, heartbeat usually ranges from 48 to 120 beats per minute, the corresponding frequency range is 0.8 — 2.0 Hz, while respiration is 0.1 — 0.5 Hz. Physiological signatures captured by radar generally comprise a superposition of cardiac and respiratory components, which can be mathematically modeled as two sinusoidal oscillations.

$$v(t)=A_{\mathrm{H}}\sin(\omega_1 t+\theta_1)+A_{\mathrm{R}}\sin(\omega_2 t+\theta_2)+\eta(t), \tag{9}$$

where $\eta(t)$ represents noise fluctuations caused by environmental interference and body movements; θ is a constant phase shift; ω_1 and ω_2 correspond to the frequencies of heartbeat and respiration. A_{H} and A_{R} are related to the chest displacement caused by heartbeat and respiration, usually the displacement caused by heartbeat is 0.1 — 0.5 mm, while the respiration is 1 — 12 mm. Due to the differences between individuals, parameters such as amplitude and frequency of these vital signs exhibit significant differences. Therefore, researchers focus on developing advanced signal processing techniques to accurately extract and analyze individual vital signs from radar.

Each beat of the heart is driven by electrical signal propagation among myocardial cells, which can be captured through surface electrodes and converted into a graphical waveform known as an electrocardiogram (ECG). Different from ECG signals, radar-detected heartbeat signals originate from mechanical thoracic oscillations induced by cardiac activity. Although the two signal modalities differ fundamentally in their physiological mechanisms, the heartbeat cycle duration extracted from radar signals exhibits high consistency with ECG measurements[29]. This is because the chest mechanical fluctuation detected by radar signal is triggered by myocardial electrical activity reflected by ECG. Therefore, accurate extraction of heartbeat signal from radardata, particularly identification of peak points corresponding to maximal thoracic displacement, enables precise estimation of inter-beat intervals (IBIs), thereby facilitating quantitative assessment of HRV.

To effectively carry more HRV information, adjusting key radar parameters is crucial. The main parameters include chirp rate, bandwidth, and slow-time sampling rate. The chirp rate K is defined as the ratio of bandwidth B to the sweep period T_c, and it determines the radar's sensitivity to small phase changes. Since the chest displacement caused by heartbeats is extremely weak, a higher chirp rate can produce greater phase shifts, enhancing the detection capability for subtle heartbeat movements. The system bandwidth B primarily affects distance resolution, a larger bandwidth provides finer distance resolution, which helps better isolate weak vital sign signals in environments with static clutter or multipath reflections. The slow-time sampling rate F_s determines the sampling density of the heartbeat waveform along the time axis. To accurately capture heartbeat peaks and calculate millisecond-level IBIs, F_s should be maximized considering data transmission and processing burdens, to avoid ambiguity or loss in peak identification due to undersampling, which is especially critical for time-domain analysis of HRV.

1.3 Method overview

The proposed method is used for non-contact human HRV detection in clinical settings. The process of this method is shown in Fig. 3. The schematic diagrams of second derivative, signal compression, and window energy conversion mentioned in Part 2 are also reflected in Fig.3. The system architecture consists of three core modules.

1) Signal preprocessing. This stage primarily involves target localization and phase extraction. Target localization is achieved through spectrum analysis and background subtraction algorithms. Phase information is extracted frame by frame from the range bin representing human body, followed by phase unwrapping, phase differencing, and outlier noise removal to obtain original signals containing heartbeat signal.

2) Heartbeat signal feature enhancement. Enhance heartbeat signal features through second derivative, and adopt two-stage nonlinear compression to suppress noise and further highlight heartbeat features. Window energy discretization is combined with to construct a multi-level energy index space. A periodic segmentation method based on adaptive threshold discrimination was proposed. For threshold optimization, an SVM regression model integrating crest factor, sample entropy, and frequency energy ratio was established. This achieved effective noise suppression while preserving heartbeat features, laying the foundation for subsequent heartbeat cycle segmentation.

3) Estimation of heartbeat interval. Perform heartbeat cycle segmentation on the processed signal, conduct peak detection based on the derived heartbeat cycles, extract identification points to calculate heart rate intervals, and subsequently obtain HRV parameters.

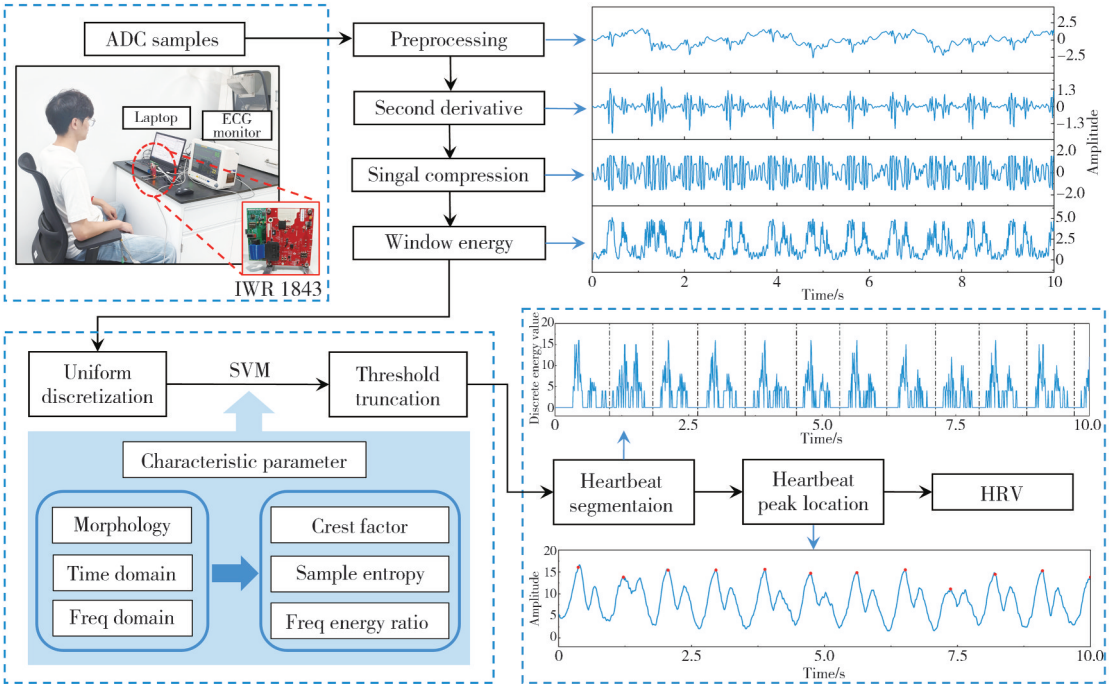

Fig. 3 Proposed signal processing block diagram

2 Proposed method

2.1 Signal preprocessing

In non-contact vital sign detection systems, the accurate determination of the target range bin is the primary step for signal extraction. The general method involves processing IF signals from FMCW radar through the following workflow. Fast Fourier transform (FFT) is performed along the fast-time dimension for each chirp signal (referred to as range FFT) to construct a range-time spectrogram matrix $\boldsymbol{X}[m,n]$. Here, $m\in[1,M]$ represents the slow-time dimension sampling points, and $n\in[1,N]$ represents the range bin index, as illustrated in Fig.2. This process maps the echo signal to the range domain, where the resolution is determined by the radar bandwidth B, satisfying $\Delta R=c/(2B)$.

In practical applications, complex indoor environments introduce static noise. Static objects such as walls and metal furniture generate strong specular reflections, producing echo energy higher than that of human targets. To address this, a background clutter elimination algorithm is used to suppress static background interference, as illustrated in Fig.4. Utilizing the characteristic that static object echoes exhibit stable energy over time while dynamic object echoes have significant energy fluctuations, the algorithm subtracts the mean value of each range bin from its corresponding elements in the range-time matrix.

This process can be expressed as

$$\hat{\boldsymbol{X}}[m,n]=\boldsymbol{X}[m,n]-\frac{1}{M}\sum_{m=1}^{M}\boldsymbol{X}[m,n]. \quad (10)$$

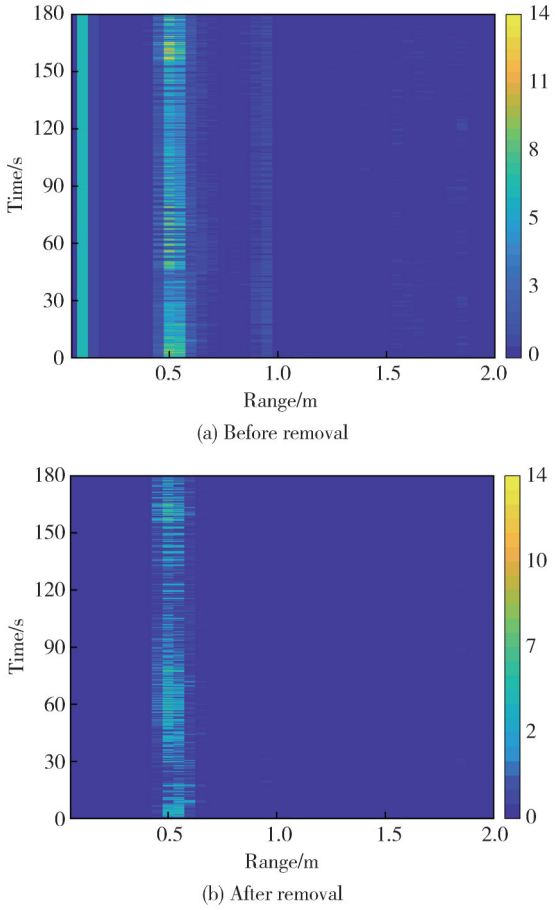

Fig. 4 Static clutter removal results

This operation effectively suppresses static clutter while preserving dynamic target echoes. Afterwards, we sum the energy of each range bin, and the range bin with the highest

echo energy value is identified as the target range bin. The phase of each frame at this range bin is then extracted and sequenced chronologically. This involves calculating the arctangent of the raw I/Q channel data to form the original discrete phase sequence $\phi(m)$ of the target. However, due to the characteristics of the arctangent function, the extracted phase may exhibit discontinuities, requiring further phase unwrapping processing.

$$\nabla\phi(m)=\begin{cases}\phi(m)-\phi(m-1)-2\pi, \phi(m)-\phi(m-1)>\pi,\\ \phi(m)-\phi(m-1)+2\pi, \phi(m)-\phi(m-1)<-\pi.\end{cases} \tag{11}$$

The resulting time-varying phase signal $\nabla\phi(m)$ may still contain residual DC offsets. To address this, a first difference operation is applied to eliminate the DC bias term.

$$V(m)=\nabla\phi(m)-\nabla\phi(m-1). \tag{12}$$

These signal preprocessing steps ensure the integrity and clarity of the signal while eliminating partial noise.

2.2 Heartbeat signal feature enhancement

After preprocessing, the radar echo signal $V(m)$ containing vital signs is obtained. To segment heartbeat cycles, the signal is first subjected to bandpass filtering with cutoff frequencies set to 0.8 — 2 Hz, aligned with the normal human heartbeat frequency range. In the filtered signal, the time-domain peak detection method is employed to identify peaks, and an initial individual heartbeat cycle window is estimated by dividing the total test duration by the number of detected peaks. Since the subject in the experimental environment remains in a relatively stable state, the heartbeat variability is minimal, allowing this window to serve as a preliminary basis for heartbeat cycle segmentation.

Since the micro-features of heartbeat are significantly stronger than respiration, and the acceleration of respiratory motion is much smaller than that of heartbeat motion, this signal is subjected to second derivative to obtain signal $x(t)$, which emphasizes the heartbeat signal by highlighting the acceleration value. The signal is normalized and then subjected to a two-stage compression algorithm to enhance signal features. During compression, there are two adjustable parameters. α represents the compression ratio, and θ represents the compression threshold. The first stage is based on a moderate compression ratio to suppress low-amplitude noise while preserving key heartbeat features, preparing for subsequent energy mapping (θ_1=0.006, α_1=5). The second stage is based on a higher compression ratio to further highlight signal features (θ_1=0.015, α_1=30), as shown in Fig.5. The equations are

$$x_c^{(1)}(t)=\begin{cases}\mathrm{sgn}(x(t))\left(\theta_1+\dfrac{|x(t)|-\theta_1}{\alpha_1}\right), & |x(t)|>\theta_1,\\ x(t), & \text{else},\end{cases} \tag{13}$$

$$x_c^{(2)}(t)=\begin{cases}\mathrm{sgn}(x_c^{(1)}(t))\left(\theta_2+\dfrac{|x_c^{(1)}(t)|-\theta_2}{\alpha_2}\right), & |x_c^{(1)}(t)|>\theta_2,\\ x_c^{(1)}(t), & \text{else}.\end{cases} \tag{14}$$

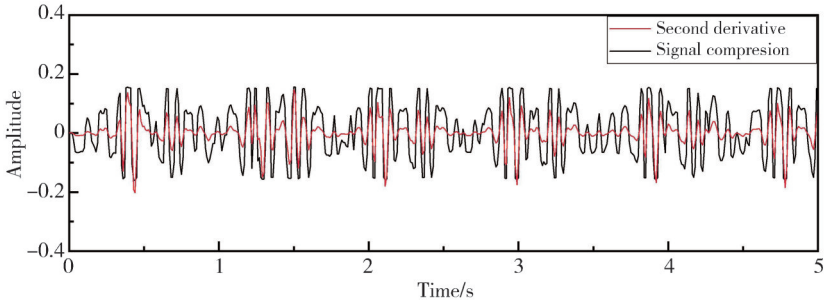

Fig. 5 Schematic diagram of signal nonlinear compression

The radar heartbeat signal after the second derivative processing exhibits distinct physiological characteristic differences. The attenuation in the amplitude of IBI signals between adjacent cardiac cycles compared to heartbeat peaks is very significant. Based on this property, an adaptive segmentation algorithm was proposed based on energy gradient and dynamic threshold determination. By quantifying the energy distribution within local windows, the algorithm accurately identifies low-energy transitional regions between heartbeats, enabling robust segmentation of continuous heartbeat cycles. Furthermore, the time-domain statistical properties of HRV parameters (such as SDNN, RMSSD) primarily depend on the sequence stability of adjacent IBIs, demonstrating strong tolerance to slight ambiguities in cycle boundaries. Therefore, accurate HRV values can be obtained provided that critical peaks are effectively preserved during the segmentation process.

After signal compression, energy mapping and discretization are performed to simplify analysis and reduce computational complexity. Calculate the window energy, then normalize and map it to a multi-level energy index.

$$E(t)=\sum_{t}^{t+W-1}\left|x_{c}^{(2)}(t)\right|^{2}, \tag{15}$$

$$C(t)=\left\lfloor(E-1)\frac{E(t)-E_{\min}}{E_{\max}-E_{\min}}\right\rfloor+1, \tag{16}$$

where W represents the window length and E represents the number of energy indices. A larger window length enhances noise resistance for signals but may excessively blur heartbeat boundaries. Considering that the typical steady-state duration of heartbeat motion is approximately 0.5 s, the window length is generally set to 10 — 15 frames. Mapping energy to multi-level indices transforms physiological features in radar signals into a highly discriminative discrete decision space, thereby providing clear boundaries for regular segmentation.

Threshold truncation is used to distinguish the noise in the stationary area from the effective heartbeat signal, where the selection of thresholds directly impacts the effect of subsequent heartbeat signals segmentation. Mean crest factor, sample entropy, and frequency energy ratio were used to assist in threshold selection and evaluate the performance of the threshold. The crest factor, also known as peak-to-average power ratio (PAPR), is defined as the ratio of a signal's peak value to its root mean square value. It quantifies the prominence of signal peaks within waveforms, thereby characterizing morphological variations in physiological signals. Sample entropy measures the complexity of time series. Lower values indicate higher self-similarity in sequences, while higher values reflect greater complexity. This metric is widely used for assessing the complexity of physiological time series and diagnosing pathological conditions. The frequency energy ratio represents the proportion of energy within a specific frequency band relative to the total spectral energy. It effectively assesses the clarity and stability of heartbeat signals. A higher frequency energy ratio typically indicates stronger energy concentration in the target frequency range and lower noise contamination. These parameters are mathematically defined as

$$Crest\,factor=\frac{\max x}{\sqrt{\frac{1}{N}\sum_{i=1}^{N}x_{i}^{2}}}, \tag{17}$$

$$Sample\,entropy(m,r,N)=-\ln\left(\frac{A}{B}\right), \tag{18}$$

$$Frequency\,energy\,ratio=\frac{E_{\mathrm{H}}}{E_{\mathrm{t}}}=\frac{\sum_{f_i\in F}\left|X(f_i)\right|^{2}}{\sum_{j=1}^{N}\left|X(f_j)\right|^{2}}, \tag{19}$$

where N is the length of the sample signal; m is the dimension of the template vector; and r represents the similarity threshold; A and B correspond to the number of matched template vector pairs in $m+1$ dimensional and m dimensional spaces, respectively; E_{H} refers to the total energy within the heartbeat frequency band F (i.e., 0.8—2 Hz); E_{t} is the total energy across the entire frequency spectrum; $X(f)$ represents Fourier transform of the signal.

The acquired data was divided into 60 sets of 60-second segments for analyzing heartbeat signal features using a SVM to predict processing thresholds. These segments were derived from 25 volunteers (18 males, 7 females) aged 23—55 years with BMI ranging from 16.9 to 28.4, including 4 underweight, 3 overweight, and 1 obese subjects to ensure physiological diversity. The dataset includes multiple samples, each consisting of three features and their corresponding processing thresholds. To enhance the nonlinear representation capability of key features, squared and cubic terms of the frequency energy ratio are incorporated. Parameters are standardized to eliminate dimensional influences and ensure training stability. The core of the support vector regression algorithm is transforming data into a high-dimensional feature space through nonlinear mapping to identify the optimal regression hyperplane. The kernel function selects radial basis function (RBF) for its strong nonlinear expression ability. Model performance is evaluated using mean squared error (MSE) and the coefficient of determination (R^2).

Experimental results demonstrate that the model exhibits strong fitting capabilities, as evidenced by MSE of 0.112 and R^2 of 0.964 2. This indicated that referencing morphological, time domain, and frequency domain characters of the signal enable effective prediction of the required truncation threshold.

2.3 Estimation of heartbeat interval

As shown in Fig. 6, heartbeat cycle segmentation is performed. First, by identifying all zero-value indices in the signal, continuous zero-value regions are detected and stored. The interval lengths between consecutive zero-value segments are calculated. The midpoint of the first identified continuous zero-value segment with a corresponding duration exceeding 50 ms is selected as the initial segmentation point. The selection of the 50 ms threshold is determined by analyzing cardiac biomechanical

properties and signal processing observations. Under conditions of the fastest heart rate observed in healthy humans, the stationary period of cardiac mechanical activity detected by radar occupies approximately one-third of the cardiac cycle. Therefore, the empirical threshold should be less than 150 ms.

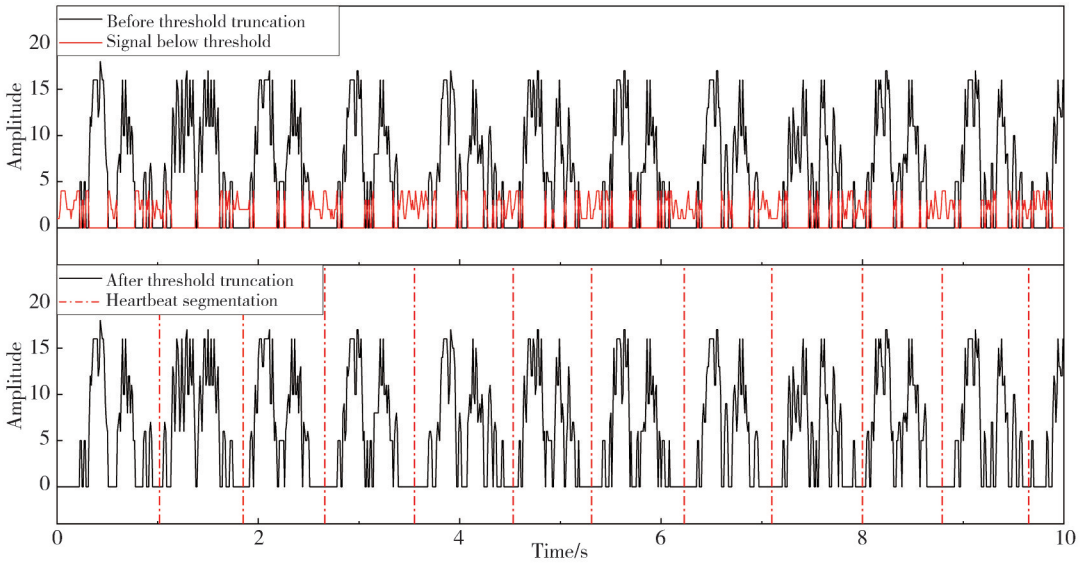

Fig. 6 Example of threshold removal and cycle segmentation

It is also observed that the energy accumulation region corresponding to actual heartbeat events does not contain consecutive zero-value segments exceeding 30 ms. Thus, setting the threshold at 50 ms ensures that segmentation points are not placed within the concentrated energy region essential for accurate heartbeat identification, while simultaneously avoiding missed cardiac cycles due to detection failures. Using the previously estimated heartbeat cycle window as the initial step size, the next segmentation point is determined by prioritizing the midpoint of continuous zero-value segments near the predicted position. If no such segment exists, the nearest zero-value point to the predicted position is selected. After determining each segmentation point, the current heartbeat cycle duration is calculated. If it meets requirements, this newly obtained cycle length is adopted as the updated step size for locating subsequent segmentation points, with this iterative process continuing to calculate all subsequent segmentation points. The flowchart of the dynamic segmentation process is shown in Fig.7.

Based on the segmentation points of heartbeat cycle boundaries obtained through time-domain segmentation, the envelope waveforms of each segmented heartbeat cycle are stored independently. Considering the presence of double-peak characteristics within typical heartbeat cycles, peak detection is performed using the first half of frames in each heartbeat cycle to avoid interference from secondary peaks during cycle alignment. Moving average is applied to eliminate glitch noise interference, and the selected point of peak time is designated as the identification point for corresponding heartbeat cycle. This dynamic segmentation-based heartbeat peak localization approach demonstrates significant advantages in resisting secondary peak interference, computational efficiency, and general applicability.

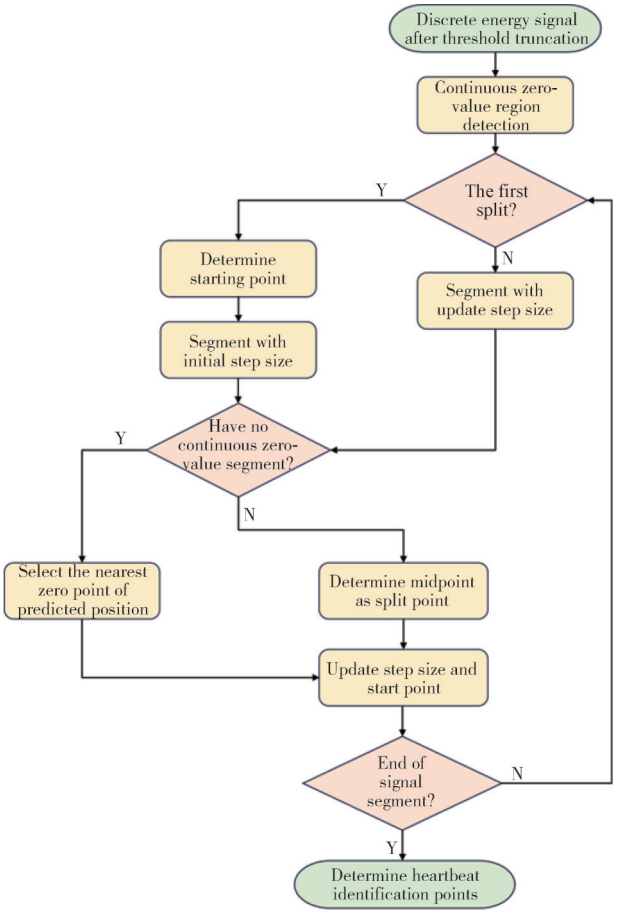

Fig. 7 Dynamic segmentation flowchart

By analyzing the extracted sequence of identification points, the intervals between adjacent heartbeat peaks can be determined. After calculating all heartbeat intervals, derived parameters such as the standard deviation of NN intervals (SDNN) and root mean square of successive differences (RMSSD) can be obtained through further calculations. These parameters reflect the stability and regularity of heart rate variability, aiding in identifying potential health risks through further analysis.

3 Results and discussion

3.1 Experimental equipment and environment

The Texas instruments IWR1843BOOST millimeter wave radar was used in conjunction with the DCA1000 EVM data capture card to transmit radar data via Ethernet. The radar was configured with a starting operating frequency of 77 GHz, a sweep bandwidth of approximately 3 GHz and a single input single output antenna configuration, operating at a slow time sampling rate of 200 Hz.

All experimental procedures were conducted in a laboratory environment. During the experiments, participants were seated in chairs positioned 40 — 80 cm from the radar antenna array, directly facing the radar. Subjects maintained a relaxed posture throughout the trials, avoiding significant torso movements while maintaining regular breathing patterns. A KF 12 electrocardiogram monitor (from Cofoe Medical Technology Co., Ltd.) served as the reference standard for validating heartbeat intervals extraction accuracy. The actual experimental setup is shown in Fig.3.

3.2 Analysis of experimental results

To further enhance accuracy and reduce computational complexity, a 30-second fixed window was implemented in the final data processing stage. This helps to dynamically adjust the truncation thresholds and segmentation step sizes. Concurrently, the SDNN and RMSSD are calculated whenever IBI data accumulates to two minutes.

Fig.8(a) shows the segmentation of heartbeat cycles and the localization of heartbeat identification points of 100 second radar heartbeat data, and synchronously compares them with ECG R-wave peaks.

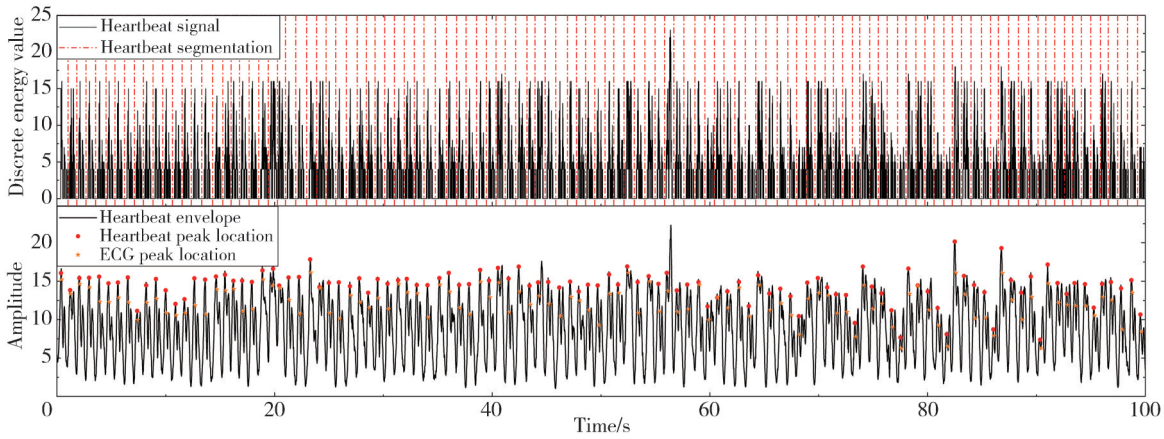

(a) Heartbeat segmentation example of 100 s and comparison of result and ECG R-wave peaks location, and comparison of ECG monitor and radar measurement results

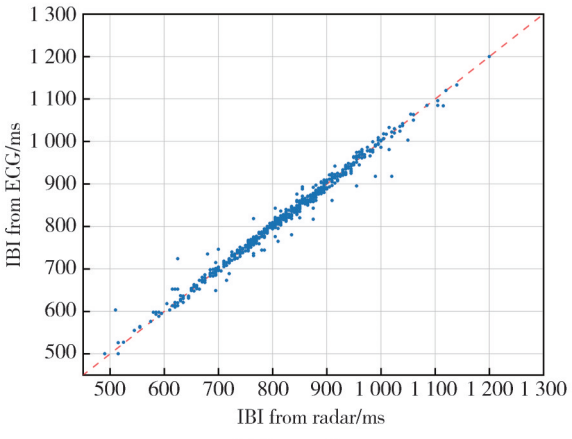

(b) Scatter diagram

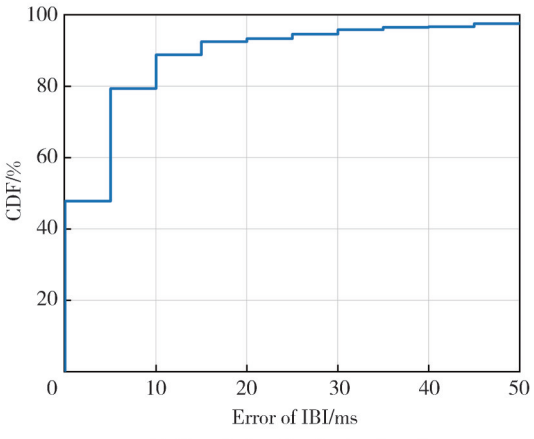

(c) Cumulative distribution function

Fig. 8 Experimental results

Although the radar-detected mechanical heartbeat peaks do not perfectly align with ECG R-wave peaks, the IBIs are calculated based on temporal differences between consecutive identification points, resulting in minimal impact on IBI computation. When two consecutive IBIs within the window exhibit excessive divergence and both deviate significantly from the window's mean IBI, the identification point is flagged as anomalous, with its adjacent IBIs excluded from statistical analysis and subsequent calculations.

In Fig.8(b), the X-axis and Y-axis represent the IBIs derivedfrom radar data and ECG monitor, respectively. Most of the points are clustered on the diagonal, indicating that the IBIs collected and processed by the radar is relatively accurate. Fig. 8(c) shows the cumulative distribution function (CDF) of the error between IBI obtained by radar processing and IBI obtained by ECG monitor, with over 92% of IBI errors confined within 20 ms. Experimental results indicate an average IBI error of 8.28 ms and RMSE of approximately 15.3 ms. Furthermore, in the comparative experiment, the conventional peak detection algorithm applied without periodic segmentation frequently experienced threshold failure, resulting in a significantly higher average IBI error of no less than 30 ms.

Table 1 shows the five-minute HRV detection results from five participants, with average heart rates ranging from 58 to 107 beats per minute, covering the typical heart rate distribution observed in the general population.

Table 1 HRV estimation results of mean IBI, SDNN, and RMSSD for five participants

No.	HRV	Result (ECG/radar)/ms	Error/ms	Relative error/%
#1	Mean IBI	801.05/**806.60**	5.55	0.69
	SDNN	51.51/**53.08**	1.57	3.05
	RMSSD	42.53/**44.33**	1.80	4.23
#2	Mean IBI	779.70/**785.98**	6.28	0.81
	SDNN	40.16/**47.05**	6.89	17.16
	RMSSD	29.34/**34.92**	5.58	19.02
#3	Mean IBI	601.12/**614.50**	13.38	2.23
	SDNN	38.05/**40.00**	1.95	5.12
	RMSSD	27.81/**32.81**	5.00	17.98
#4	Mean IBI	1 020.62/**1 009.91**	10.71	1.05
	SDNN	62.73/**63.42**	0.69	1.10
	RMSSD	45.30/**49.14**	3.84	8.48
#5	Mean IBI	826.01/**812.17**	13.84	1.68
	SDNN	57.22/**59.38**	2.16	3.77
	RMSSD	37.16/**42.59**	5.43	14.61

The radar was configured 40 cm from participants to measure three core HRV parameters: mean IBI, SDNN, and RMSSD. Experimental results demonstrate that the mean IBI errors measured by the radar remained are below 15 ms, with the maximum of only 13.84 ms and an average relative error of 1.29%. Subject #3 exhibites the maximum relative error at only 2.23%. Furthermore, average errors of SDNN and RMSSD are 2.65 ms and 4.33 ms, respectively.

To evaluate the impact of measurement distance on the performance of radar HRV detection, comparative testing was conducted with the radar positioned at 40 cm and 80 cm from participants under controlled experimental conditions. As shown in Fig. 9, the median absolute IBI errors in boxplots for the long-distance group exhibit a 3 — 6 ms elevation compared to the short-distance group, but remain below 15 ms.

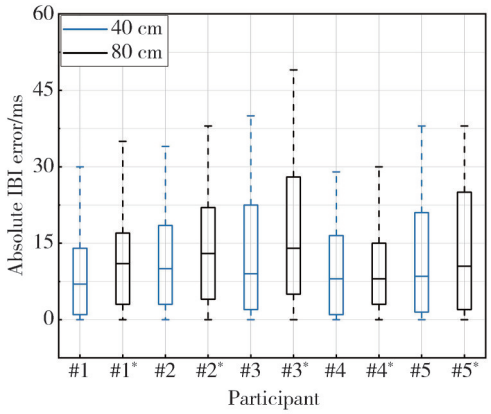

Fig. 9 Boxplot comparing IBI test errors for five participants at different distances. Boxes represent errors of 25% — 75%. Dashed lines represent extreme error, and horizontal lines in boxes represent median error

However, elongated box ranges indicate nonlinear degradation in elevated outlier proportions in the long-distance group are observed, which may attributable to signal attenuation and ambient spatial noise interference. Overall, the change in distance did not have a significant impact on the average results, indicating that this method can meet the detection needs of general medical diagnosis and experimental conditions.

Table 2 presents the comparison of the detection performance of the method proposed in this study with that of other related studies.

Table 2 Performance comparison of similar studies

Ref.	Radar frequency/GHz	Mean IBI RMSE/ms	Average SDNN error/ms	Average RMSSD error/ms
23	77	21.8	5.46	—
24	77	14.9	3.54	6.55
29	77	26.1	6.44	6.43
This paper	77	15.3	2.65	4.33

Although the other methods can also achieve relatively accurate HRV detection, they may suffer from issues such as complex signal processing procedures. These limitations could potentially restrict their flexibility and efficiency in

practical applications. Our study demonstrates excellent performance in detecting mean IBI, SDNN, and RMSSD while emphasizing streamlined algorithm design to simplify processes, making it more suitable for dynamic monitoring and clinical applications.

4 Conclusions

A non-contact HRV detection method was proposed based on FMCW radar, achieving high-precision IBI and derived parameter extraction through efficient multistage signal processing. The core algorithm employed second derivative and two-stage nonlinear threshold compression to enhance heartbeat feature. The designed dynamic energy gradient segmentation algorithm significantly enhanced the SNR of heartbeat peaks while reducing computational complexity. Additionally, an adaptive threshold optimization mechanism was implemented by developing an SVM regression model incorporating morphological-temporal-spectral features. Under standard detection distance (40 cm), the system demonstrates RMSE of 15.3 ms for mean IBI, with average errors of 2.65 ms and 4.33 ms for SDNN and RMSSD, respectively. In the distance adaptability test, the system maintained robust detection performance. The experimental results showed that this detection method could effectively suppress the influence of respiratory harmonics and environmental noise on IBI extraction. Future work will focus on multi-objective HRV monitoring algorithms and further enhance detection reliability in dynamic environments.

Acknowledgement

This work was supported by National Natural Science Foundation of China (Nos. 62320106002, U22A2014); National Key Research and Development Program of China (No. 2021YFA1401103); 2022 Wuxi Taihu Talent Program: Innovative Leading Talent Team (No.1096010241230120); Fundamental Research Funds for Central Universities (No. 1322050205250910); Wuxi Municipal Basic Research Project (No.K20241026).

Declaration of conflicting interests

The authors have no conflict of interests related to this publication.

References

[1] SHAFFER F, GINSBERG J P. An overview of heart rate variability metrics and norms. Frontiers in Public Health, 2017, 5: 258.

[2] THAYER J F, AHS F, FREDRIKSON M, et al. A Meta-analysis of heart rate variability and neuroimaging studies: implications for heart rate variability as a marker of stress and health. Neuroscience and Biobehavioral Reviews, 2012, 36(2): 747-756.

[3] COPPOLA A, CONTE S, PASTORE D, et al. Multifractal heart rate value analysis: a novel approach for diabetic neuropathy diagnosis. Healthcare, 2024, 12(2): 234.

[4] OLIVEIRA JÚNIOR I G, CAMELO L V, MILL J G, et al. Job stress and heart rate variability: findings from the ELSA-Brasil cohort. Psychosomatic Medicine, 2019, 81(6): 536-544.

[5] JEYHANI V, MAHDIANI S, PELTOKANGAS M, et al. Comparison of HRV parameters derived from photoplethysmography and electrocardiography signals// 2015 37th Annual International Conference of the IEEE Engineering in Medicine and Biology Society (EMBC), August 25-29, 2015, Milan, Italy. New York: IEEE, 2015: 5952-5955.

[6] PATEL S, PARK H, BONATO P, et al. A review of wearable sensors and systems with application in rehabilitation. Journal of NeuroEngineering and Rehabilitation, 2012, 9: 21.

[7] WILSON A N, GUPTA K A, KODURU B H, et al. Recent advances in thermal imaging and its applications using machine learning: a review. IEEE Sensors Journal, 2023, 23(4): 3395-3407.

[8] MOÇO A V, STUIJK S, HAAN G. New insights into the origin of remote PPG signals in visible light and infrared. Scientific Reports, 2018, 8: 8501.

[9] BEECKMAN S, BADHWAR S, LI Y L, et al. Heart-carotid pulse-wave velocity via laser-doppler vibrometry as a biomarker for arterial stiffening: a feasibility study. Physiological Measurement, 2025, 46(4): 045006.

[10] SUN S, ZHANG M L, GAO C H, et al. MEMS ultrasonic fingertip heart rate sensor. IEEE Sensors Journal, 2022, 22(21): 20285-20292.

[11] YANG F, HE S, SADANAND S, et al. Contactless measurement of vital signs using thermal and RGB cameras: a study of COVID 19-related health monitoring. Sensors, 2022, 22(2): 627.

[12] MANZAR S, BHAT R. Feasibility of handheld ultrasound to assess heart rate in newborn nursery. Resuscitation, 2022, 179: 78-82.

[13] GE Y, TAHA A, SHAH S A, et al. Contactless WiFi sensing and monitoring for future healthcare - emerging trends, challenges, and opportunities. IEEE Reviews in Biomedical Engineering, 2023, 16: 171-191.

[14] EBRAHIM M P, TOM N, REDOUTE J-M, et al. A low-frequency portable continuous wave radar system for vital signs monitoring. IEEE Sensors Journal, 2023, 23(8): 8876-8886.

[15] PAN T, GUO Y, GUO W, et al. Detection of vital sign based on UWB radar by a time domain coherent accumulation method. IEEE Sensors Journal, 2023, 23(15): 17054-17063.

[16] ANTOLINOS E, GRAJAL J. Comprehensive comparison

of continuous-wave and linear-frequency-modulated continuous-wave radars for short-range vital sign monitoring. IEEE Transactions on Biomedical Circuits and Systems, 2023, 17(2): 229-245.
[17] WANG Y, LIU H, XIANG W, et al. A novel non-contact respiration and heartbeat detection method using frequency-modulated continuous wave radar. IEEE Sensors Journal, 2024, 24(7): 10434-10446.
[18] XUE W, WANG R, LIU L, et al. Accurate multi-target vital signs detection method for FMCW radar. Measurement, 2023, 223: 113715.
[19] WU E K, FAN Q G, LI M C, et al. Non-contact monitoring of human cardiorespiratory activity during sleep using FMCW millimeter wave radar. Measurement, 2025, 242: 116144.
[20] TAYARANIAN HOSSEINI S M A, AMINDAVAR H. A new Ka-band doppler radar in robust and precise cardiopulmonary remote sensing. IEEE Transactions on Instrumentation and Measurement, 2017, 66(11): 3012-3022.
[21] HU W, ZHAO Z Y, WANG Y F, et al. Noncontact accurate measurement of cardiopulmonary activity using a compact quadrature doppler radar sensor. IEEE Transactions on Biomedical Engineering, 2014, 61(3): 725-735.
[22] WANG H Y, CHEN J B, ZHANG D H, et al. Contactless radar heart rate variability monitoring via deep Spatio-temporal modeling//2024 IEEE International Conference on Acoustics, Speech and Signal Processing (ICASSP), April 14-19, 2024, Seoul, Korea. New York: IEEE, 2024: 111-115.
[23] YUAN S, FAN S, DENG Z, et al. Heart rate variability monitoring based on doppler radar using deep learning. Sensors, 2024, 24(7): 2026.
[24] HAN X, ZHAI Q, ZHANG N, et al. A real-time evaluation algorithm for noncontact heart rate variability monitoring. Sensors, 2023, 23(15): 6681.
[25] ZHANG B B, ZHANG D H, LI Y D, et al. Monitoring long-term cardiac activity with contactless radio frequency signals. Nature Communications, 2024, 15(1): 10598.
[26] SU Y L, CHEN P. Cluster and expansion algorithm for moving object point cloud based on millimeter-wave radar. Journal of Test and Measurement Technology, 2024, 38(2): 170-178.
[27] GRIFFITHS H D. New ideas in FM radar. Electronics & Communication Engineering Journal. 1990, 2(5): 185-194.
[28] WALDSCHMIDT C, HASCH J, MENZEL W. Automotive radar-from first efforts to future systems. IEEE Journal of Microwaves, 2021, 1(1): 135-148.
[29] PETROVIC V L, JANKOVIC M M, LUPSIC A V, et al. High-accuracy real-time monitoring of heart rate variability using 24 GHz continuous-wave doppler radar. IEEE Access, 2019, 7: 74721-74733.
[30] WANG F Y, ZENG X L, WU C SH, et al. mmHRV: contactless heart rate variability monitoring using millimeter-wave radio. IEEE Internet of Things Journal, 2021, 8(22): 16623-16636.

基于自适应周期分割和峰值提取的非接触式雷达HRV监测方法

高翊轩[1], 朱新星[1], 李明潮[1], 武恩康[1], 顾晓峰[1], 王 琮[2], 喻 甜[1*], 梁峻阁[1,3,4*]

1. 江南大学 集成电路学院, 江苏 无锡 214122;
2. 哈尔滨工业大学 电子与信息工程学院, 黑龙江 哈尔滨 150001;
3. 光云大学 RFIC中心, 韩国 首尔 01897;
4. 汉阳大学 医学与数字工程系, 韩国 首尔 04763

摘 要: 心率变异性(HRV)作为评估自主神经系统功能的关键指标, 在心血管疾病筛查和情绪监测等领域具有重要价值。传统的接触式测量方法虽精度高, 但存在舒适性差、依从性低等问题。本文提出一种基于调频连续波(FMCW)雷达的非接触式HRV监测方法, 其核心创新在于自适应周期分割与峰值提取技术。该方法关键优势包括: 1) 利用心跳能量集中特性, 有效抑制运动伪影和呼吸谐波干扰; 2) 采用自适应分割实现在不同生理状态下的精准心跳周期识别, 解决时变差异问题; 3) 基于离散能量信号和形态-时域-谱特征的支持向量机(SVM)模型自适应调整阈值, 在维持精度的同时降低计算复杂度。其它方法主要通过算法对雷达信号进行整体的处理并统一获取心跳间期, 这种方式可能会产生计算复杂度高、动态适应性较差的问题。相比之下, 该方法的精度要显著高于传统的整体信号处理方法, 且计算复杂度更低。实验表明, 系统的平均心搏间期(IBI)误差为8.28 ms(均方根误差为15.3 ms), 相较传统整体寻峰方法降低了约66%。SDNN和RMSSD平均误差分别为2.65 ms和4.33 ms。超过92%以上的IBI误差控制在20 ms内。距离适应性测试表明, 虽然远距离测量精度略有下降(<6 ms), 但整体检测性能在不同距离下均保持稳定。本研究为非接触式HRV检测提供了一种新的估计算法, 为未来的健康监测提供了新的思路。

关键词: 心率变异性; 调频连续波雷达; 周期分割; 自适应阈值; 非接触监测

引用格式: GAO Yixuan, ZHU Xinxing, LI Mingchao, et al. Non-contact radar-based HRV monitoring method using adaptive cycle segmentation and peak extraction. Journal of Measurement Science and Instrumentation, 2025, 16(2): 161-172. DOI: 10.62756/jmsi.1674-8042.2025016